Research Square

Preprints are preliminary reports that have not undergone peer review.
They should not be considered conclusive, used to inform clinical practice,
or referenced by the media as validated information.

Toolpath strategy for evaluating the coefficient of friction in the incremental sheet forming process

Antonio Formisano

aformisa@unina.it

Universita degli Studi di Napoli Federico II https://orcid.org/0000-0002-4909-8315

Research Article

Keywords: Incremental sheet forming, Coefficient of friction, Toolpath, Forming forces, Finite element analysis.

Posted Date: November 6th, 2026

DOI: https://doi.org/10.21203/rs.3.rs-11162677/v1

License: This work is licensed under a Creative Commons Attribution 4.0 International License.
Read Full License

Abstract

Owing to its inherent flexibility, low tooling costs, and enhanced formability, incremental sheet forming is particularly suitable for the rapid manufacturing of high-value-added, small-batch, and customized complex sheet components. However, the tribological conditions at the tool/sheet interface play a crucial role in governing material deformation. The presence of highly localized contact pressures adds significant complexity to the interpretation and modelling of frictional behaviour within the process. The aim of the present study is to evaluate the coefficient of friction between the forming tool and the sheet in the incremental sheet forming process. To this end, a flat-head forming tool is employed, and a dedicated toolpath is developed. The parameter under investigation is measured through an in-depth understanding of the typical issues affecting incrementally formed components and a careful interpretation of the forming force signals. Finite element analyses support the results from the experimental campaign.

Introduction

Sheet forming processes are among the most widely used techniques for producing finished components in many industries, particularly in the aerospace [1], automotive [2], and household sectors [3]. Conventional sheet forming operations, such as deep drawing or stamping, are predominantly carried out at room temperature using mechanical presses equipped with dedicated dies, enabling high throughput for large-scale production runs [4]. However, the elevated costs associated with die manufacturing, press setup, and process integration render these technologies inefficient for limited-batch production or the fabrication of geometrically customized components.

To overcome these constraints, incremental sheet forming (ISF) has been introduced as a highly adaptable and economically advantageous forming methodology. In ISF, a tool typically characterized by low complexity and reduced cost follows a numerically controlled toolpath along different axes over a rigidly clamped sheet blank. The tool induces incremental, localized plastic deformation in successive layers, progressively generating the target geometry without the need for a dedicated die [5]. Owing to the small, localized tool/sheet contact zone, ISF inherently requires lower forming forces compared to conventional stamping. This deformation mechanism promotes enhanced formability, often achieving strain levels significantly beyond those attainable with traditional press forming.

Extensive experimental and numerical investigations have demonstrated the suitability of ISF for lightweight metallic alloys, particularly aluminum, titanium, and various stainless steel grades, due to their favorable strain-hardening response under localized deformation conditions [6, 7]. More recently, research activities have shifted toward the processing of non-metallic materials, including thermoplastic polymers and composite laminates, highlighting the technique’s potential for multi-material and hybrid manufacturing applications [8].

Friction represents a key phenomenon that strongly influences the flow behaviour of deformed materials during the sheet forming processes, with effects on the surface quality, geometric accuracy and force

demand. Friction modelling studies further confirm that lubrication conditions significantly affect frictional behaviour and material flow in sheet metal forming [9]. Relatively to ISF, the forming tool continuously slides over the sheet surface under high contact pressure, generating friction and wear that directly affect forming forces, tool life, and the surface integrity of the parts [10]. Insufficient lubrication can promote adhesion, galling, and pronounced tool marks, particularly when forming high-strength alloys [11]. Moreover, lubrication conditions interact with key process parameters, thereby influencing forming forces and dimensional accuracy; then, a proper understanding of the frictional properties of sheet materials is crucial for designing manufacturing processes and tooling systems.

From a tribological standpoint, lubrication performance is strongly governed by lubricant chemistry and the mechanisms underlying boundary film formation. Classical tribology establishes that boundary lubrication films develop through the adsorption of polar molecules onto metallic surfaces under high contact pressures [12]. In industrial forming operations, oil-in-water emulsions are frequently employed due to their combined cooling and lubricating capabilities, which arise from the synergistic action of base oils, surfactants, and corrosion inhibitors [13]. Vegetable-oil-based lubricants have gained increasing interest as environmentally sustainable alternatives to mineral-based oils due to their biodegradability and advantageous tribological characteristics. The polar ester functional groups present in vegetable oils facilitate strong adsorption onto metallic surfaces, promoting the formation of resilient boundary lubrication films even under severe contact conditions [14].

Considerable efforts have been dedicated to developing more effective lubrication strategies for ISF, since an appropriate lubrication significantly decreases friction and enhances surface finish [15]. A promising and sustainable approach is Minimum Quantity Lubrication (MQL), capable of improving tribological performance while drastically reducing lubricant consumption compared with conventional flood-cooling methods [16]. Alternative lubrication approaches have also been investigated; for instance, graphite grease-based lubricants exhibit superior lubricant retention at the tool/sheet interface and contribute to a reduction in forming forces during ISF operations [17], while vegetable-oil-based nanolubricants incorporating SiO_2 nanoparticles have been shown to improve boundary lubrication behaviour and enhance wear resistance [18]. Moreover, dedicated systems, such as roller-ball lubrication tools, have been proposed to maintain a continuous lubrication regime during heat-assisted ISF, mitigating lubrication loss at elevated temperatures [19].

The feature that better represents the friction conditions and directly affects the accuracy of predictive or finite element (FE) simulation models [20] is the coefficient of friction (*COF*). In metal forming, its interpretation is not simple, due to high local pressures that intensify adhesion and plowing effects; this evaluation is further complicated in hot sheet metal forming, where adhesion significantly contributes to total contact resistance [21].

Different papers have provided an overview of the methods developed over time to characterize friction conditions in both conventional and ISF. Concerning ISF, the *COF* has been evaluated by assessing direct and indirect tribological testing techniques or calculated by combining theoretical and experimental

approaches. The continuous contact between the forming tool and the sheet leads to complicated friction conditions, with a difficult evaluation of the relationship between the forming parameters and the *COF* [22]. Consider, for example, that different evaluation strategies involve the measure of the forming forces but the *COF* results difficult to calculate precisely because the sheet plane forces contain not only the friction contribution [23] but also disturbing factors such as indentation, flattening, or thrust on the lateral walls of the components [24, 25]; moreover, a significant limitation of these approaches is that they provide only average *COF* values that do not allow the assessment of the actual frictional resistance [26]. Furthermore, some investigations have provided for the manufacture of components that do not resemble typical ISF parts like, for example, U-shaped grooves through a zigzag toolpath [10].

Considering above, this study experimentally evaluates the *COF* at the tool/sheet interface by developing a dedicated toolpath strategy that allows for the manufacture of typical ISF parts and considers the actual friction conditions. This evaluation employs the forming forces that a flat-head forming tool transfers to the material sheet for the manufacture of square frusta. FE simulations follow the experimental campaign, and their results support the goodness of the *COF* procedure. The study highlights the importance of a deepen knowledge of all the issues that interest incrementally formed components to a careful evaluation of the feature under examination.

Materials and Methods

Square frusta with fixed wall angles are manufactured by ISF, using a C.B. Ferrari high-speed four-axis vertical machining centre. The process is carried out at room temperature on Makrolon polycarbonate sheets (supplied by Bayer), 2.9 mm in thickness. From the engineering stress–strain curves (see, for example, the curves for 2 mm thick sheets in [27]), this material shows linear and nonlinear elastic behaviour, shear-band forming and post-yield behaviour with necking and its propagation corresponding to strain softening, typical of amorphous thermoplastics [28]; the Young's modulus, the strain at failure and the yield stress are equal to 2.3 GPa, 60%, and 60 MPa, respectively.

The sheets are clamped into a fixture, having a square working area with a side of 100 mm, and deformed by the progressive action of a forming tool. To obtain a well-defined contact surface between the tool and the sheet that allows for easier interpretation of the force data, a non-rotating stainless-steel stylus with a flat head is chosen; Fig. 1 reports a CAD model of the tool and its main geometric features. To reduce the probability of failures, the sheets are lubricated with mineral oil for cold forming [29].

Figure 2 shows a partial, non-scale representation of the toolpath developed in this study, based on an in-plane strategy with constant vertical step (Δz) and wall angle (α) [30]; a view in the XY- and XZ-plane is represented in Fig. 2a and Fig. 2b, respectively. The distance of the starting point (labelled as a) along the horizontal axes (X and Y) from the Z-axis is labelled as d, while the total vertical displacement is z_{MAX}, as indicated below in the text. Only the first two complete z-levels are shown, separated by Δz; they are representative of all subsequent pairs of z-levels.

Each *z*-level involves contouring (four segments) followed by eight diagonal segments; the sequence of segments described during the toolpath is reported in Table 1, while Table 2 describes the types of segments. The *vertical* segments correspond to the vertical step and guarantee the progressive and incremental deformation of the sheet. The *contour* segments constitute the contouring that defines the shape of the components. The *diag_1* and *diag_2* segments go from the vertices to the sides and from the sides to the vertices of a *z*-level, respectively (note that the points along the sides divide them into a 1 : 3 ratio); along the central part of these segments, the *COF* is expected to be evaluated, as there should be no disturbing factors (or, however, minimized) [24, 25]. The two consecutive *z*-levels are described in opposite directions (see the arrows in Fig. 2) to reduce twisting to zero [31], so as observed by the authors in previous works on metal [32] and polycarbonate ISF parts [33].

Table 1
Sequence of segments described during the toolpath

Description	**Segment**
First vertical step	ab
First *z*-level	bc - cd - de - eb - bf - fe - eg - gd - dh - hc - ci - ib
Second vertical step	bl
Second *z*-level	lm - mn - no - ol - lp - po - oq - qn - nr - rm - ms - sl

Table 2
Type of segments described during the toolpath

Type	**Segment**
vertical	ab - bl
contour	bc - cd - de - eb - lm - mn - no - ol
diag_1	bf - eg - dh - ci - lp - oq - nr - ms
diag_2	fe - gd - hc - ib - po - qn - rm - sl

The toolpaths are described at a nominal speed of 1000 mm/min. To test different working conditions, two sets of process parameters are chosen:

- d = 40 mm, Δz = 2 mm, α = 30°, and z_{MAX} = 16 mm (#1_toolpath);
- d = 45 mm, Δz = 1 mm, α = 45°, and z_{MAX} = 20 mm (#2_toolpath).

One moment (M_Z) and three forces (F_X, F_Y, and F_Z) are recorded at 50 Hz by the K-MCS10 multicomponent sensor (HBK World, Southfield, MI, USA), equipped with the QuantumX MX840B data acquisition system and the Catman Easy AP software V5.6.1. From the combination of the force

components, the force acting in the sheet plane (F_{XY}) and the total force (F_{TOT}) are obtained. Then, the *COF* is calculated as the ratio between F_{XY} and F_Z.

FE simulations follow the experimental tests; the general-purpose commercial software MSC Marc/Mentat 2025.2, based on an implicit non-linear solver, is employed.

The numerical model, developed in the Mentat preprocessor environment, consists of the sheet and the forming tool. The square sheet (side of 100 mm) is discretized using 2500 structural 3-D solid shell elements (2.0 × 2.0 mm^2; thickness of 2.9 mm), while the tool is modelled as a rigidwall. The sheet material is described using an isotropic elastic-plastic model, based on the properties reported above. Boundary conditions are defined by assigning a structural fixed displacement to the peripheral nodes of the sheet (X = Y = Z = 0) to simulate the clamping frame.

The simulations are performed setting the *COF* previously evaluated by the experimental procedure. The toolpath is imposed by prescribing controlled translational motions to the tool along X, Y and Z directions. The simulations are run setting a constant time step of 0.01 s. FE results are analysed using Mentat software.

Results and Discussion

The components do not experience tearing for both toolpaths; this result was predictable, since the wall angles chosen are significantly lower than the maximum one obtained through formability tests, equal to 80° [33]. However, the components formed using the #1_toolpath show clear technological marks due to more severe working conditions. In this regard, Fig. 3a highlights the indentations left by the tool, which are not as evident as when the process is carried out using the #2_toolpath (Fig. 3b). For the purposes of assessing the *COF*, these phenomena are undoubtedly sources of disturbance, which is why the considerations that follow in the rest of the text relate to the tests conducted with #2_toolpath, unless otherwise explicitly stated.

Figure 3 also highlights that the components do not show any twisting, as a result of the choice of the toolpath that alternates in anticlockwise and clockwise directions for each *z*-level; in so doing, the twist generated in one *z*-level is almost entirely recovered in the subsequent one [8]. This is confirmed by the graph in Fig. 4, representing M_Z for the toolpath corresponding to *z*-levels of 9 and 10 mm. It can be clearly seen that the moments for the two *z*-levels are almost mirror images of each other and therefore, overall, for each pair of them, the effects of these moments tend to cancel each other out.

For evaluating the *COF*, it is important to analyse the trend of F_Z and F_{XY} forces. In this regard, Fig. 5 shows this trend for the same time window as Fig. 4.

The figure shows that the force peaks correspond to the points of the toolpath. The highest peaks are at the end points of the *vertical* segments (b and l points of ab and bl segments), since they are vertex points after the vertical step; indentation mainly affects these points.

The next four peaks are progressively lower as the flattening during contouring is reduced each time; at the same time, F_{XY} forces are high because they are affected by the thrust on the lateral walls, typical of *contour* segments.

The next height segments (*diag_1* and *diag_2*, alternatively) are those who are least affected by the disturbing effects; this is clear by observing the values reached by F_{XY} forces. The ones that have the lowest peaks are the *diag_1* segments, which end at the sides. However, the most interesting segments for evaluating the *COF* are the *diag_2* segments, as they are further away from the contour segments in their central part, reflecting on the lowest F_Z and F_{XY} values. Therefore, for each *z*-level, the average of F_Z and F_{XY} values is measured within a range of ± 0.1 s around the minimum points of the *diag_2* segments. From their ratio, and from the ratio between F_Z and the contact area (equal to 50.2 mm^2), the *COF* and the contact pressure *P* are evaluated, respectively.

The graph in Fig. 6 reports the minimum value of the *COF* for each *z*-level, as a function of the corresponding *P* value (to consider the stabilised region of the forming process, the data related to the first *z*-level are not considered). A decreasing trend of the *COF* with increasing *P* is observed; this behaviour may be associated with a change in the lubrication regime, as reported in [34]. Moreover, this approach overcomes the limitations of methods that provide only average *COF* values, which may lead to an inaccurate assessment of the actual frictional resistance.

A numerical simulation is performed by defining the *COF* as a function of the *z*-level. In particular, its trend corresponds to the dashed line shown in Fig. 7, while the points represent the experimental data. As an example, Fig. 8 shows the equivalent von Mises stress distribution at the end of the FE simulation, highlighting the deformed sheet and the geometrical surfaces representing the forming tool.

To validate the proposed *COF* procedure, a numerical-experimental comparison is performed in terms of F_{TOT}. Figure 9 presents this comparison for the toolpath corresponding to *z*-levels of 5 mm (Fig. 9a) and 15 mm (Fig. 9b), representing two different friction conditions. The results show good agreement between experimental and numerical data in both cases, confirming the suitability of the *COF* procedure for describing the tool/sheet friction interaction.

Conclusions

This study presents an experimental procedure for evaluating the coefficient of friction at the tool/sheet interface in incremental sheet forming processes. The procedure is based on a dedicated toolpath strategy and a detailed analysis of the forming forces exerted by a flat-head tool on the sheet. Tests on polycarbonate sheets highlight the importance of a thorough understanding of the typical issues affecting incrementally formed components, which may act as disturbing factors in the evaluation of friction. The results show that the proposed procedure enables the assessment of actual friction conditions, which are influenced by the working parameters. In the present case, the coefficient of friction can be expressed as a function of the tool/sheet contact pressure. Numerical analysis

performed after the experimental phase further supports the validity of the proposed approach. Future work will extend the experimental campaign to different materials and lubricants and will focus on advanced numerical modelling to more accurately simulate the incremental sheet forming process. In particular, iterative procedures for assigning the coefficient of friction as a function of the actual working conditions will be developed.

Declarations

Declaration of generative AI and AI-assisted technologies in the writing process

During the preparation of this work the author used Edu GPT in order to improve its readability. After using this tool/service, the author reviewed and edited the content as needed and takes full responsibility for the content of the publication.

Competing Interests

The author has no relevant financial or non-financial interests to disclose.

Funding

The author declares that no funds, grants, or other support were received during the preparation of this manuscript.

Author Contributions

Study conception and design, material preparation, data collection, and analysis were performed by Antonio Formisano, as well as the writing of the manuscript.

Data Availability Statement

Data sets generated during the current study are available from the corresponding author on reasonable request.

References

1. Cao J, Banu M (2020) Opportunities and challenges in metal forming for lightweighting: Review and future work. J Manuf Sci Eng Trans ASME 142. https://doi.org/10.1115/1.4047732
2. Yi HL, Sun L, Xiong XC (2018) Challenges in the formability of the next generation of automotive steel sheets. Mater Sci Technol (United Kingdom) 34:1112–1117.

https://doi.org/10.1080/02670836.2018.1424383
3. Li Q, Xu C, Gao S et al (2022) Research on the forming quality of clinched joint for dissimilar sheet metal. Int J Adv Manuf Technol 119:2945–2959. https://doi.org/10.1007/s00170-021-08602-1
4. Simoncelli A, Buglioni L, Martínez Krahmer D, Sánchez Egea A (2025) Effects of machine compliance on forming accuracy and forces in SPIF of AISI 430. Int J Adv Manuf Technol 1–14. https://doi.org/10.1007/s00170-025-15854-8
5. Ben Said L (2022) The incremental sheet forming; technology, modeling and formability: A brief review. Proc Inst Mech Eng Part E J Process Mech Eng 236:2729–2755. https://doi.org/10.1177/09544089221093306
6. Kumar R, Kumar V, Kumar A (2023) A Review on Effect of Computer-Aided Machining Parameters in Incremental Sheet Forming. In: Handbook of Flexible and Smart Sheet Forming Techniques: Industry 4.0 Approaches. wiley, pp 29–58
7. Ortiz M, Penalva M, Iriondo E, López de Lacalle LN (2020) Investigation of Thermal-Related Effects in Hot SPIF of Ti–6Al–4V Alloy. Int J Precis Eng Manuf - Green Technol 7:299–317. https://doi.org/10.1007/s40684-019-00038-z
8. Formisano A, De Fazio D, Langella A et al (2025) Comparison between cold incremental and stretch forming of flax fiber-reinforced polypropylene composites. Int J Adv Manuf Technol 142:1559–1569. https://doi.org/10.1007/s00170-025-17158-3
9. Joun MS, Park MC, Heo Y, Kim DH (2025) A Review of Friction and Lubricant in Metal Forming. Lubricants 13
10. Lu B, Fang Y, Xu DK et al (2014) Mechanism investigation of friction-related effects in single point incremental forming using a developed oblique roller-ball tool. Int J Mach Tools Manuf 85:14–29. https://doi.org/10.1016/J.IJMACHTOOLS.2014.04.007
11. Zavala JMD, Martínez-Romero O, Elías-Zúñiga A et al (2021) Study of friction and wear effects in aluminum parts manufactured via single point incremental forming process using petroleum and vegetable oil-based lubricants. Mater (Basel) 14. https://doi.org/10.3390/ma14143973
12. Hsu SM, Gates RS (2005) Boundary lubricating films: Formation and lubrication mechanism. In: Tribology International. Elsevier, pp 305–312
13. Ratoi-Salagean M, Spikes HA, Rieffe HL (1997) Optimizing film formation by oil-in-water emulsions. Tribol Trans 40:569–578. https://doi.org/10.1080/10402009708983694
14. Quinchia LA, Delgado MA, Reddyhoff T et al (2014) Tribological studies of potential vegetable oil-based lubricants containing environmentally friendly viscosity modifiers. Tribol Int 69:110–117. https://doi.org/10.1016/j.triboint.2013.08.016
15. Van Sy L, Van Viet M (2022) Influence of lubricants and lubricating methods on surface roughness in the two-point incremental sheet forming process. Int J Adv Manuf Technol 121:1365–1372. https://doi.org/10.1007/s00170-022-09435-2
16. Kumar S, Kumar R, Singh S et al (2022) A comprehensive study on minimum quantity lubrication. Mater Today Proc 56:3078–3085. https://doi.org/10.1016/j.matpr.2021.12.158

17. Xu C, Li Y, Wang Z et al (2020) The influence of self-lubricating coating during incremental sheet forming of TA1 sheet. Int J Adv Manuf Technol 110:2465–2477. https://doi.org/10.1007/s00170-020-06013-2
18. Taheri R, Kosasih B, Zhu H, Tieu AK (2017) Surface film adsorption and lubricity of soybean oil in-water emulsion and triblock copolymer aqueous solution: A comparative study. Lubricants 5. https://doi.org/10.3390/lubricants5010001
19. Gupta AK, Tandon P (2025) Impact of continuous lubricating roller-ball tool on forming characteristics in incremental sheet forming with heat-assistance. Proc Inst Mech Eng Part L J Mater Des Appl. https://doi.org/10.1177/14644207251385096
20. Ndip-Agbor E, Smith J, Ren H et al (2016) Optimization of relative tool position in accumulative double sided incremental forming using finite element analysis and model bias correction. Int J Mater Form 9:371–382. https://doi.org/10.1007/s12289-014-1209-4
21. Trzepiecinski T, Lemu HG (2020) Recent developments and trends in the friction testing for conventional sheet metal forming and incremental sheet forming. Met (Basel) 10:47. https://doi.org/10.3390/met10010047
22. Zimeng Y, Xiaoming L, Shenli W et al (2023) Influence of forming parameters on friction coefficient in single point incremental forming process. Ferroelectrics 609:20–40. https://doi.org/10.1080/00150193.2023.2198950
23. Xu D, Wu W, Malhotra R et al (2013) Mechanism investigation for the influence of tool rotation and laser surface texturing (LST) on formability in single point incremental forming. Int J Mach Tools Manuf. https://doi.org/10.1016/j.ijmachtools.2013.06.007
24. Asghar J, Lingam R, Shibin E, Reddy NV (2014) Tool path design for enhancement of accuracy in single-point incremental forming. Proc Inst Mech Eng Part B J Eng Manuf 228:1027–1035. https://doi.org/10.1177/0954405413512812
25. Durante M, Formisano A, Langella A, Capece Minutolo FM (2009) The influence of tool rotation on an incremental forming process. J Mater Process Technol 209:4621–4626. https://doi.org/10.1016/j.jmatprotec.2008.11.028
26. Szpunar M, Szawara P, Myśliwiec P, Ostrowski R (2023) Influence of Input Parameters on the Coefficient of Friction during Incremental Sheet Forming of Grade 5 Titanium Alloy. Adv Mech Mater Eng 40:113–123. https://doi.org/10.7862/rm.2023.12
27. Durante M, Formisano A, Boccarusso L, Langella A (2020) Influence of cold-rolling on incremental sheet forming of polycarbonate. Mater Manuf Process 35:328–336. https://doi.org/10.1080/10426914.2020.1726946
28. Cao K, Ma X, Zhang B et al (2010) Tensile behavior of polycarbonate over a wide range of strain rates. Mater Sci Eng A 527:4056–4061. https://doi.org/10.1016/j.msea.2010.03.088
29. Beșliu-Băncescu I, Slătineanu L, Dodun O, Nagîț G (2021) Influence of Lubrication and Cooling on the Quality of Single-Point Incremental Forming Parts of Polycarbonate Sheets. J Manuf Mater Process 5:75. https://doi.org/10.3390/JMMP5030075

30. Popp GP, Racz SG, Breaz RE et al (2024) State of the Art in Incremental Forming: Process Variants, Tooling, Industrial Applications for Complex Part Manufacturing and Sustainability of the Process. Mater (Basel) 17:5811. https://doi.org/10.3390/ma17235811
31. Formisano A, Boccarusso L, De Fazio D, Durante M (2024) Effects of toolpath on defect phenomena in the incremental forming of thin polycarbonate sheets. Int J Adv Manuf Technol 133:4957–4966. https://doi.org/10.1007/s00170-024-14047-z
32. Jeswiet J, Micari F, Hirt G et al (2005) Asymmetric Single Point Incremental Forming of Sheet Metal. CIRP Ann 54:88–114. https://doi.org/10.1016/S0007-8506(07)60021-3
33. Durante M, Formisano A, Lambiase F (2018) Incremental forming of polycarbonate sheets. J Mater Process Technol 253:57–63. https://doi.org/10.1016/j.jmatprotec.2017.11.005
34. Figueiredo L, Ramalho A, Oliveira MC, Menezes LF (2011) Experimental study of friction in sheet metal forming. Wear 271:1651–1657. https://doi.org/10.1016/j.wear.2011.02.020

Figures

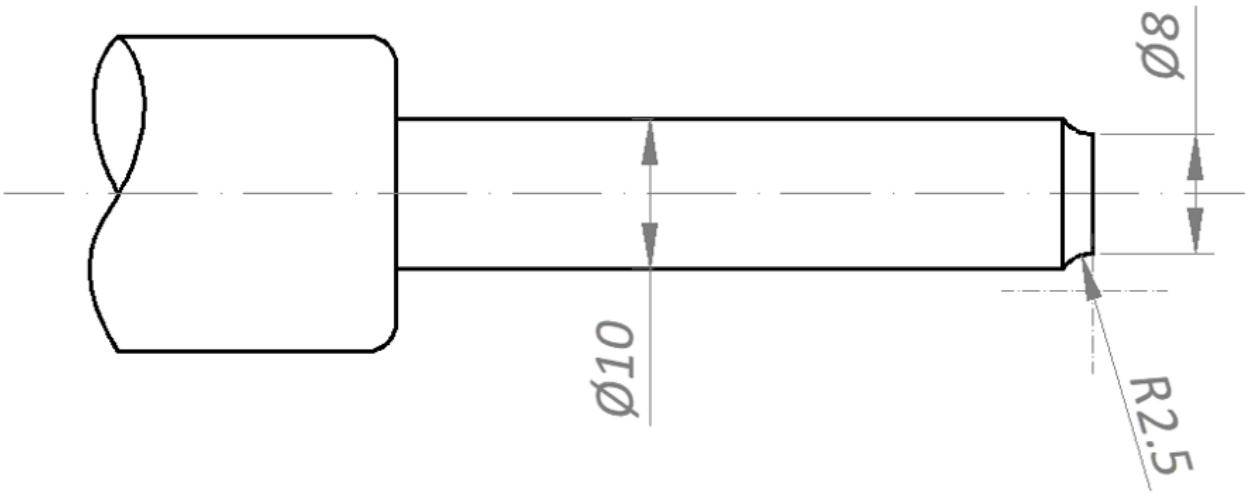


Figure 1

CAD representation of the forming tool

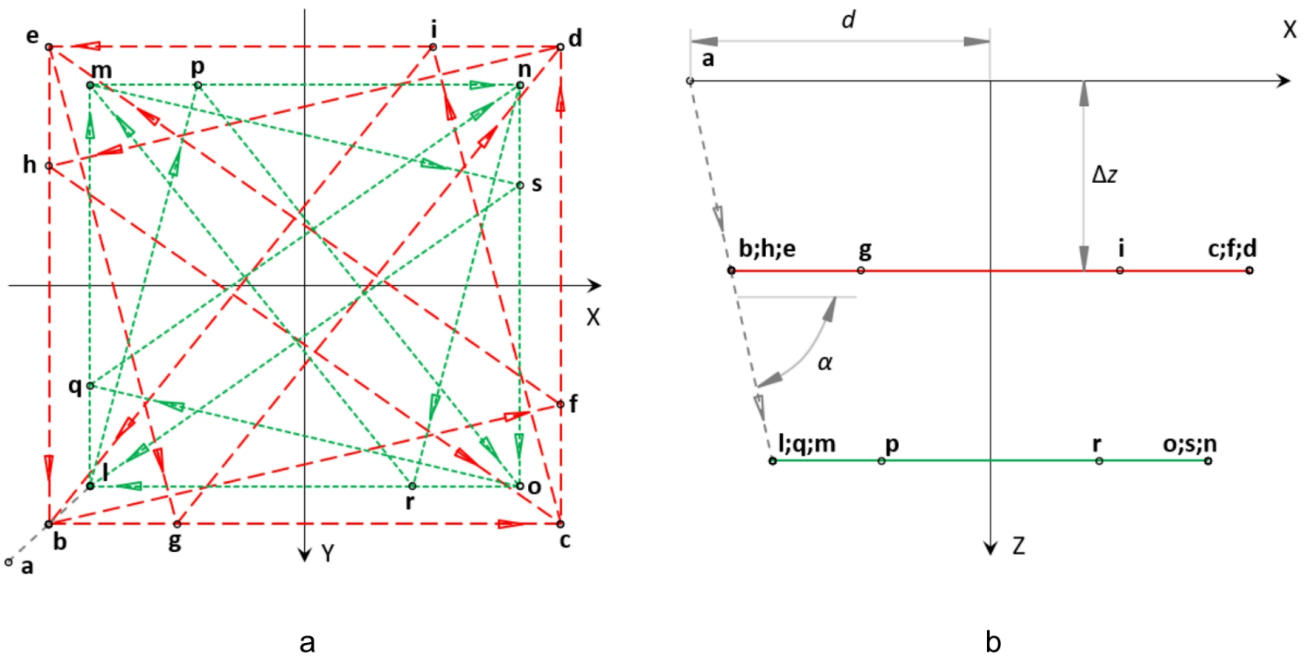


Figure 2

Representation of the toolpath strategy: (a) XY-plane view; (b) XZ-plane view

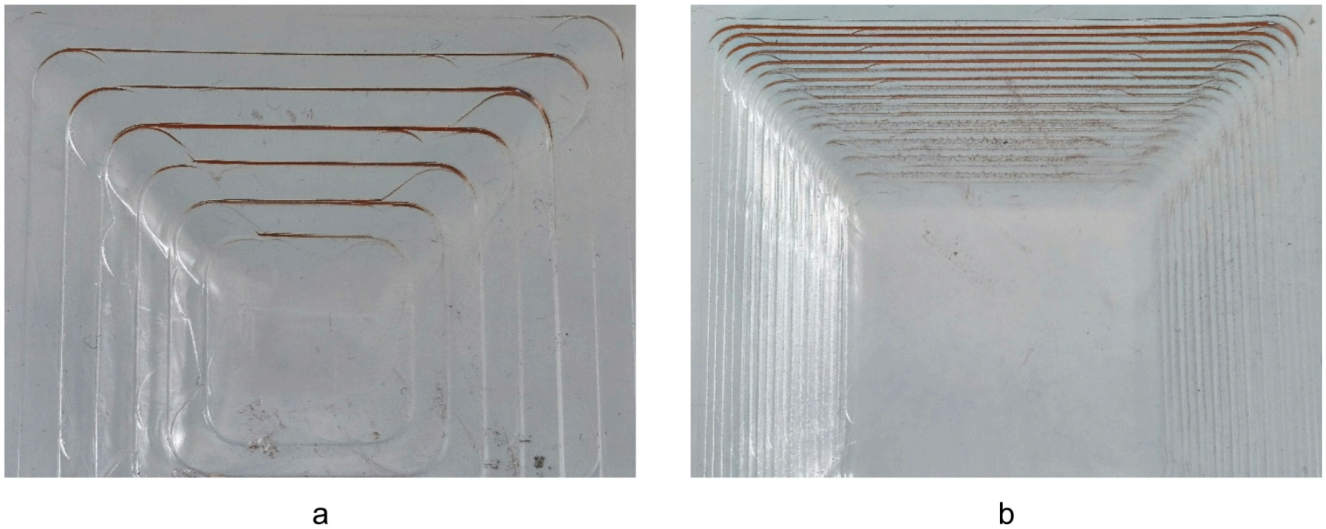


Figure 3

Components obtained by: (a) #1_toolpath; (b) #2_toolpath

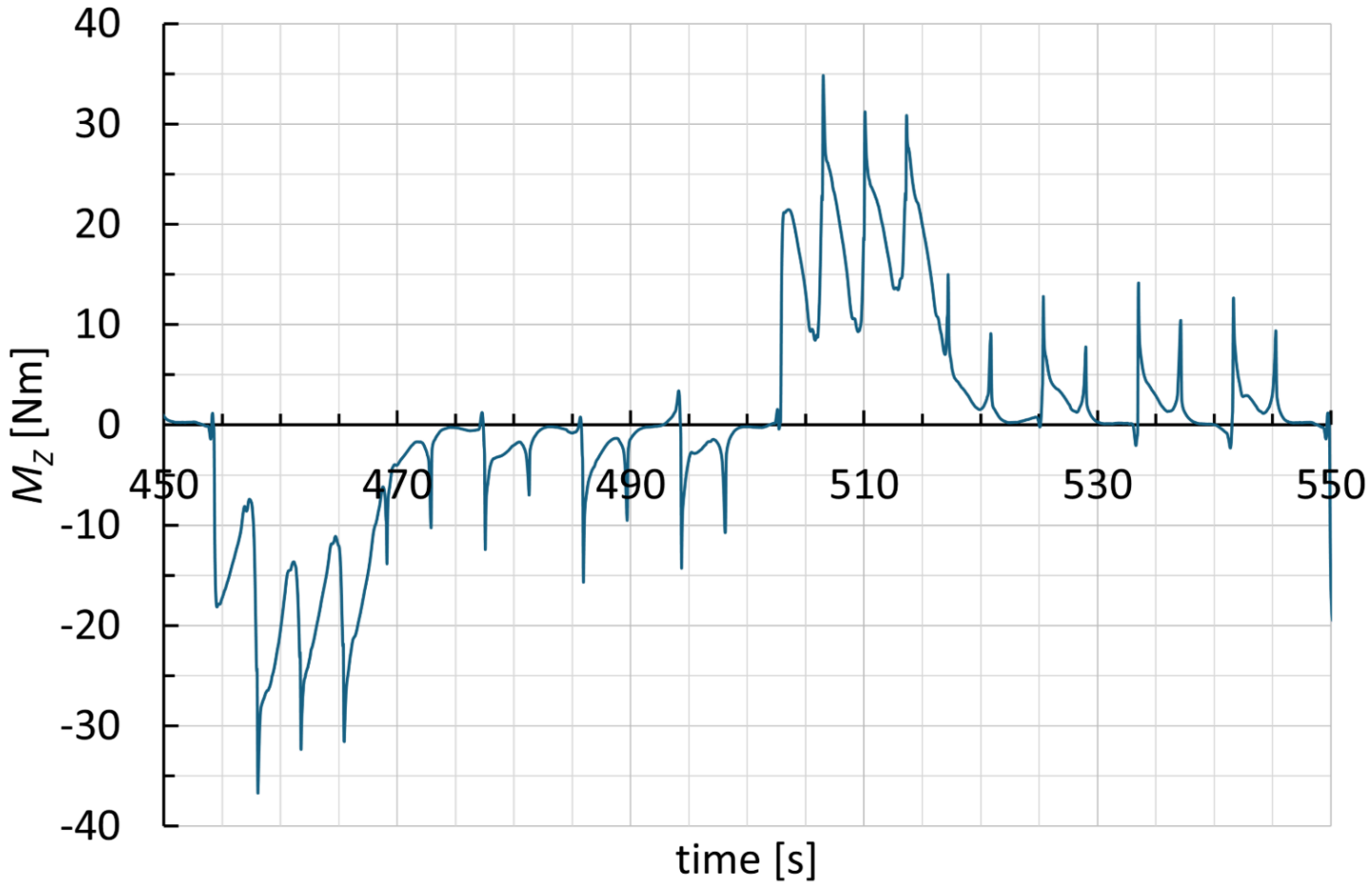


Figure 4

Trend of M_Z for the toolpath corresponding to z-levels of 9 and 10 mm

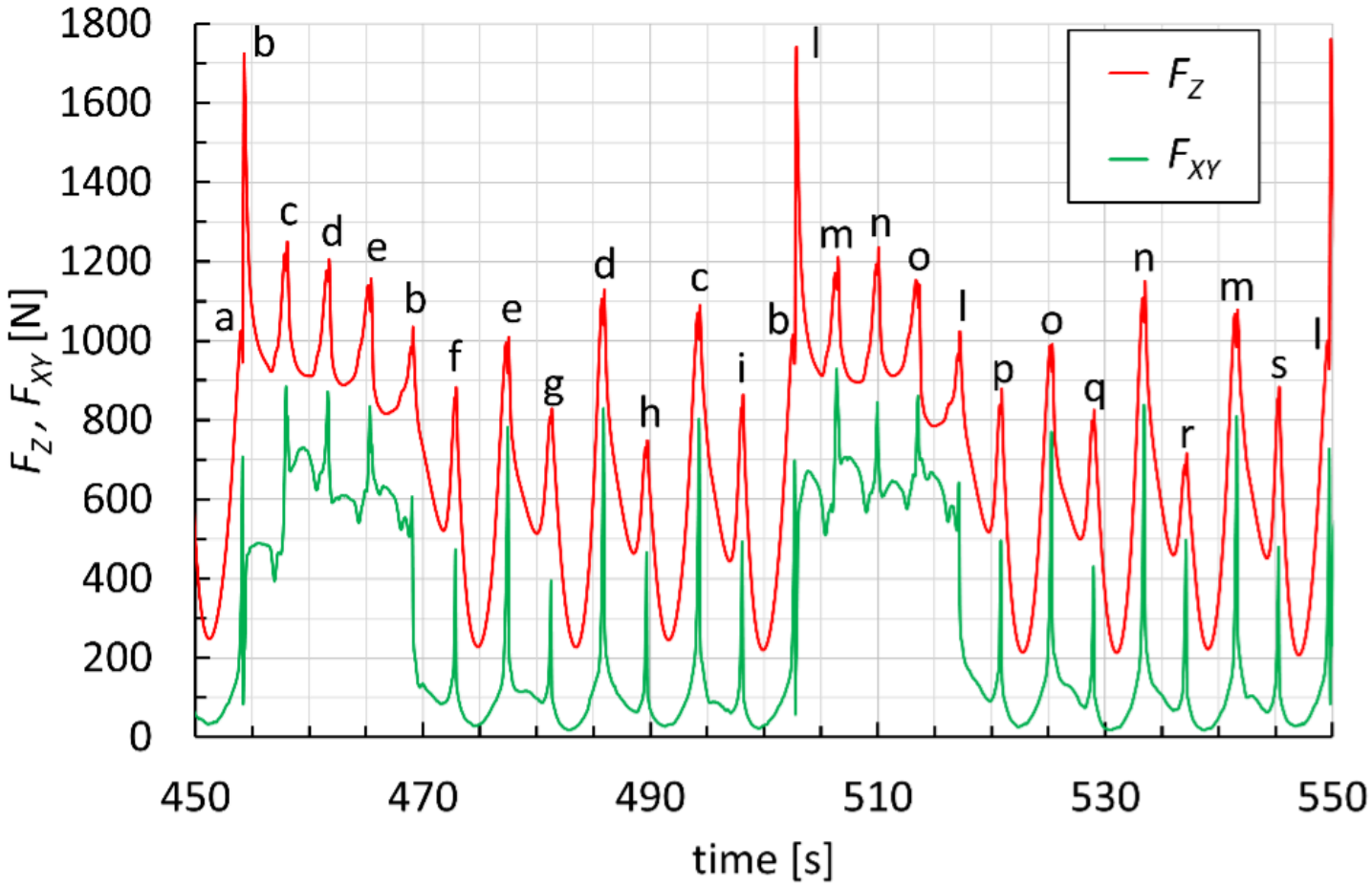


Figure 5

Trend of F_Z and F_{XY} for the toolpath corresponding to z-levels of 9 and 10 mm

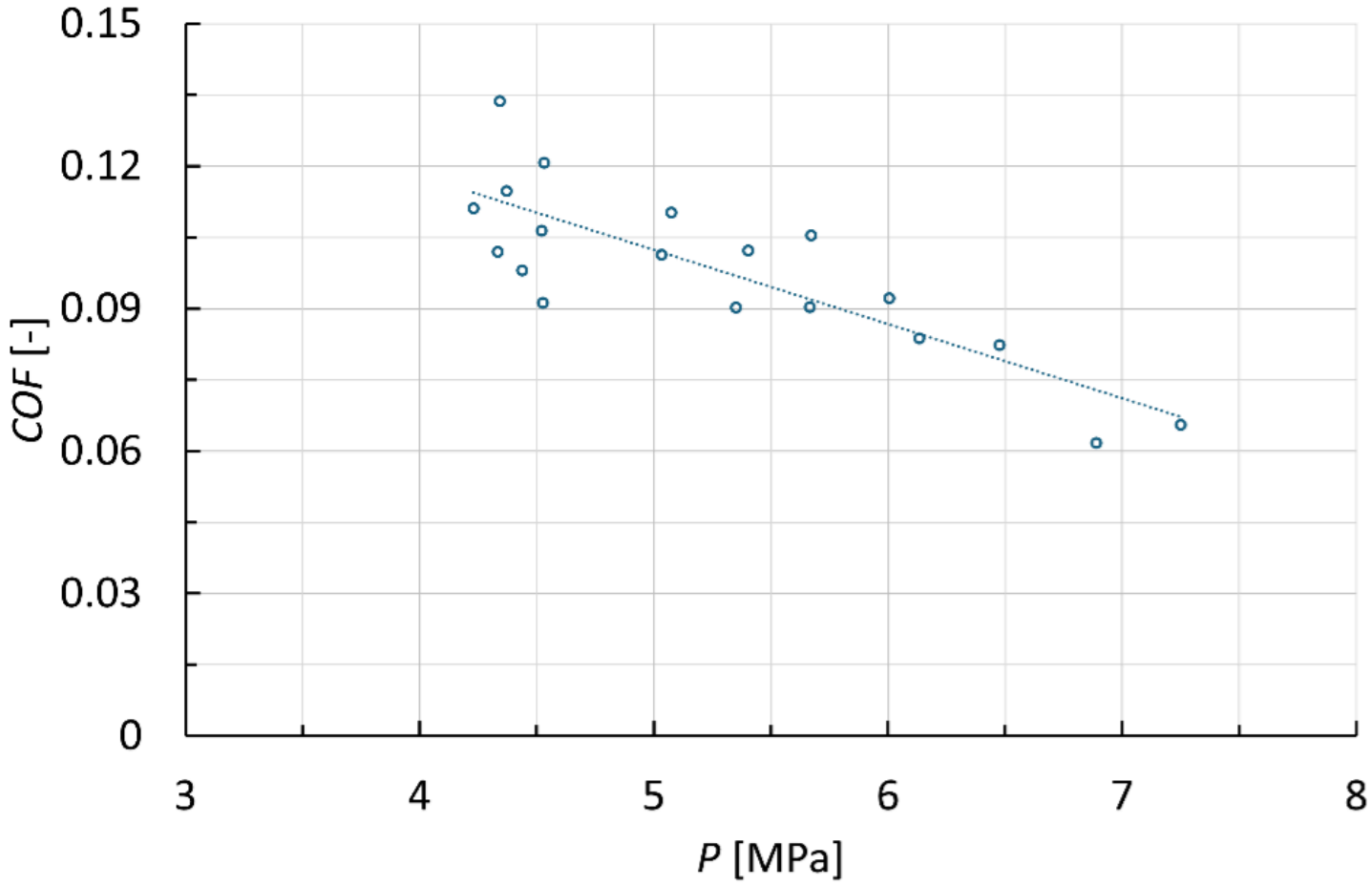


Figure 6

Trend of the COF as a function of P

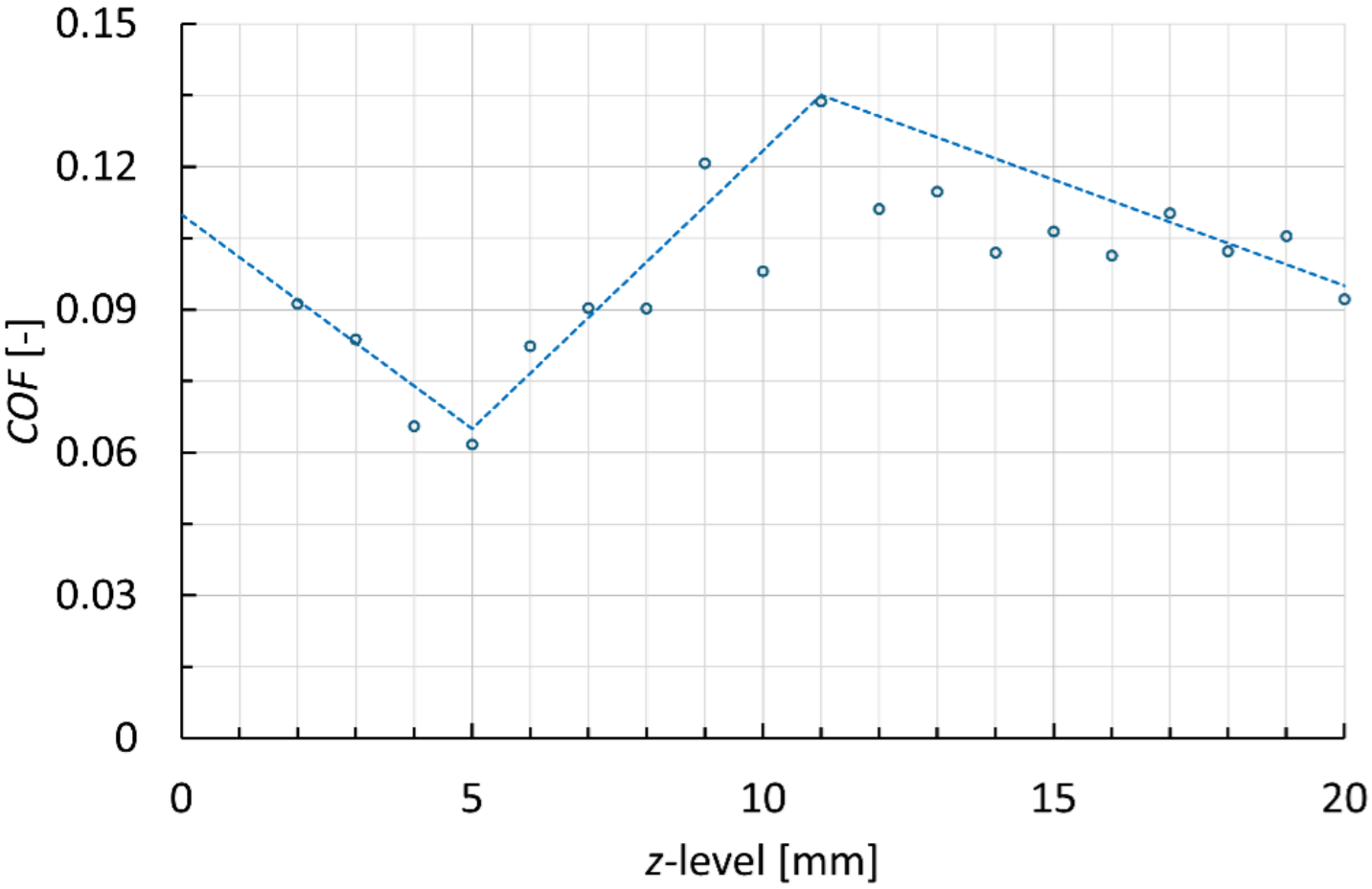


Figure 7

Trend of the COF as a function of z-level

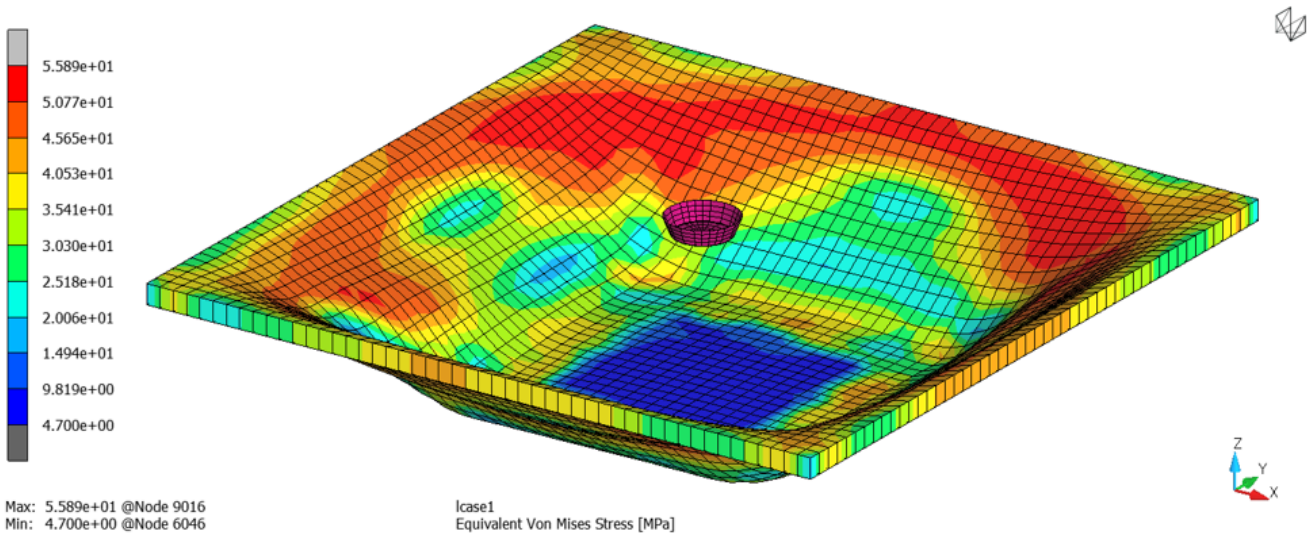


Figure 8

FE equivalent von Mises stress distribution at the end of the simulation

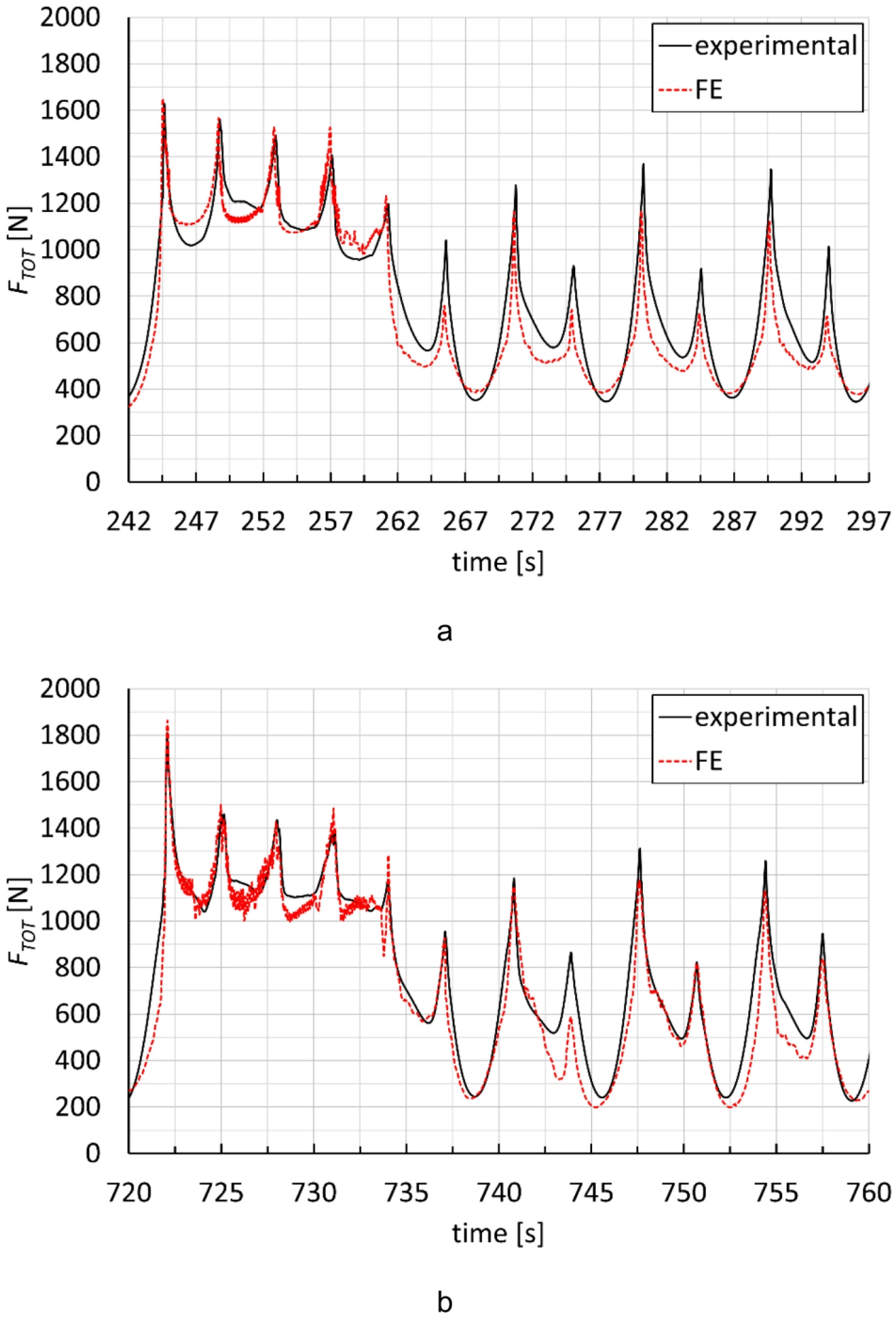


Figure 9

Experimental and FE trend of F_{TOT} for the toolpath corresponding to z-level of: (a) 5 mm; (b) 15 mm